2026, Scienceline Publication
World's Veterinary Journal
World Vet J, 16(2): 418-435.
ISSN 2322-4568

DOI: https://dx.doi.org/10.54203/scil.2026.wvj40
PII: S232245682600040-16

Antimicrobial Activity of Nano-encapsulated *Salvia Officinalis* against Methicillin-Resistant *Staphylococcus aureus* and *Acinetobacter Baumannii*

Bakary Chorr[1]*, James Kimotho[2], and Mourine Kangogo[3]

[1]*Department of Molecular Biology and Biotechnology, Pan African University for Basic Science, Technology and Innovation, Nairobi, P.O. Box 62000-00200, Kenya*
[2]*Innovation and Technology Transfer Division, Kenya Medical Research Institute, Nairobi, P.O. Box 54840-00200, Kenya*
[3]*Department of Medical Microbiology, Jomo Kenyatta University of Agriculture and Technology, Nairobi, P. O. Box 62000-00200, Kenya*

*Corresponding author's Email: bchorr10@gmail.com

ORIGINAL ARTICLE
Received: March 21, 2026
Revised: April 23, 2026
Accepted: May 20, 2026
Published: June 30, 2026

ABSTRACT

Antimicrobial resistance represents a global health burden requiring innovative therapeutic strategies. The antibacterial properties of *Salvia officinalis* (*S. officinalis*) are attributed to its bioactive compounds. The present study aimed to investigate the antimicrobial activity of nano-encapsulated *S. officinalis* leaf extract against methicillin-resistant *Staphylococcus aureus* (MRSA) and *Acinetobacter baumannii* (*A. baumannii*). The crude extract of *S. officinalis* was subjected to methanolic extraction, and the resulting methanolic fraction was analyzed through phytochemical screening. Phytocompounds were identified using gas chromatography-mass spectrometry (GC-MS), and their potential mechanisms of action were evaluated *in silico*. The *S. officinalis* extract was nano-formulated using chitosan and characterized by scanning electron microscopy (SEM), Fourier transform infrared spectroscopy, and UV-visible spectroscopy. Antibacterial activity of the nano-formulation against MRSA and *A. baumannii* was assessed using agar well diffusion, broth microdilution, and minimum bactericidal concentration analysis. Qualitative phytochemical analysis revealed the presence of flavonoids, alkaloids, tannins, saponins, and terpenoids. The GC-MS analysis demonstrated 15 peaks, representing 14 distinct compounds, with one compound (3,7,11,15-tetramethyl-2-hexadecen-1-ol) eluting at two retention times. Chitosan nanoparticle formation was confirmed by an absorption peak near 290 nm. The functional groups of chitosan nanoparticles included hydroxyl (-OH) and amide (-NH_2) groups, along with C–H, C–N, C–O, and P=O stretching. The SEM imaging exhibited relatively homogeneous, well-dispersed, spherical nanoparticles. The antimicrobial efficacy of *S. officinalis* chitosan nanoparticles was concentration-dependent, reaching maximum inhibition zones of 21 ± 0.5 mm against MRSA and 17 ± 1.5 mm against *A. baumannii* at 500 µg/mL. Additionally, susceptibility testing revealed minimum inhibitory concentrations of 62.5 µg/mL and 125 µg/mL, and minimum bactericidal concentrations of 125 µg/mL and 500 µg/mL against MRSA and *A. baumannii*, respectively. Molecular docking analysis indicated that phytocompounds within the methanolic extract exhibited binding affinity toward penicillin-binding protein 2a (PBP2a) and the carbapenem-associated outer membrane protein (CarO). The interactions between the phytochemicals and protein targets indicated that binding to catalytic sites could inhibit the function of these resistance-associated proteins, potentially reducing antibiotic degradation. The biosynthesized *S. officinalis* chitosan nanoparticles exhibited strong antimicrobial activity against multidrug-resistant bacterial isolates, supporting their potential as antimicrobial agents.

Keywords: *Acinetobacter baumannii*, Antimicrobial resistance, Methicillin-resistant *Staphylococcus aureus*, Nanoparticle, *Salvia officinalis*

INTRODUCTION

Antimicrobial resistance (AMR) represents a significant global health challenge, largely attributed to the misuse and overuse of antibiotics across human and veterinary medicine, leading to the emergence of resistant microorganisms (Ahmed et al., 2024). Globally, it is estimated that direct deaths attributed to AMR exceeded 1.2 million in 2019, and without sufficient preventive measures, this number was expected to rise to almost 10 million deaths by 2050 (Salam et al., 2023).

The rapid emergence of antimicrobial drug-resistant bacteria is a growing global concern (WHO, 2022). Methicillin-resistant *Staphylococcus aureus* (MRSA) is a well-characterized strain that exhibits reduced susceptibility to β-lactam antibiotics, including methicillin and related compounds, and has become a prevalent cause of community-acquired infections (Ali et al., 2017). The MRSA is a significant source of serious infections in humans and animals, and it is a major public health threat (Omoshaba et al., 2020). *Staphylococcus*-related infections, particularly MRSA, predominantly affect immunocompromised individuals (Obanda et al., 2022). *Acinetobacter baumannii* (*A. baumannii*) is a clinically important opportunistic pathogen frequently associated with hospital-acquired infections globally and

To cite this paper: Chorr B, Kimotho J, and Kangogo M (2026). Antimicrobial Activity of Nano-encapsulated *Salvia Officinalis* against Methicillin-Resistant *Staphylococcus aureus* and *Acinetobacter Baumannii*. *World Vet. J.*, 16(2): 418-435. DOI: https://dx.doi.org/10.54203/scil.2026.wvj40

notable for its multidrug resistance, posing a major health concern (Castillo-Ramírez et al., 2025). The World Health Organization has ranked *A. baumannii* as the top-priority bacterial pathogen urgently requiring new antibiotics (WHO Bacterial Priority Pathogens List, 2024).

Salvia officinalis (*S. officinalis*) is a perennial aromatic shrub classified within the Lamiaceae family (Ezema et al., 2024). Although *S. officinalis* is native to the Mediterranean basin and regions of the Middle East, its cultivation has expanded globally due to its medicinal and culinary significance (Ghorbani and Esmaeilizadeh, 2017). In traditional medicine, *S. officinalis* has been utilized for treating a wide range of ailments, including neurological disorders such as seizures and tremors, gastrointestinal conditions such as ulcers and diarrhea, metabolic disorders including hyperglycemia, as well as inflammatory diseases such as gout and rheumatism (Ghorbani and Esmaeilizadeh, 2017). Additionally, sage (*S. officinalis*) is recognized for its diverse pharmacological properties, such as sedative, antimicrobial, antioxidant, antitumor, and antihypertensive effects (Ghorbani and Esmaeilizadeh, 2017). Sage has been applied in the management of different conditions, including excessive sweating, cardiovascular diseases, chronic bronchitis, asthma, renal dysfunction, liver cirrhosis, dysmenorrhea, insomnia, infantile colic, and dyspepsia (Ezema et al., 2024).

Nanotechnology is significantly transforming modern pharmacognosy (Devi et al., 2026). Nanotechnology offers a novel and promising approach to improve medicinal plant systems (Devi et al., 2026). Nanotechnology has transformed herbal medicine by improving the bioavailability and effectiveness of phytocompounds (Kathole et al., 2025). Advancements in plant-based medicine have demonstrated that herbal remedies hold significant potential for treating currently incurable disorders (Tiwari et al., 2024). Among the most notable attributes of herbal medicines employing nanotechnology-based delivery systems is the ability to transform compounds with limited solubility, poor absorption, and instability into promising medicines (Dewi et al., 2022). Nanoparticles (NPs) are materials with dimensions ranging from 1 to 100 nm and play a crucial role in biosensing technologies, particularly in enhancing signal transduction, sensitivity, and specificity when used in electrode modifications (Esfandiari et al., 2025). Metal NPs such as gold and silver are widely applied in medicine due to their antimicrobial, anticancer, and drug delivery capabilities, enabling targeted therapy and improved therapeutic efficiency (Rahdari et al., 2023). Nanotechnology is changing medical diagnostics, treatments, and disease prevention, using powerful, innovative tools (Patel et al., 2024). Ongoing investigations and collaboration among many fields could lead to greater treatment outcomes, lower healthcare costs, and new generations of customized and accurate medicines (Kazi et al., 2025). Thus, the present study aimed to evaluate the antimicrobial activity of nano-encapsulated *S. officinalis* against MRSA and *A. baumannii*.

MATERIALS AND METHODS

Ethical approval

Ethical approval for the present study was obtained from Mount Kenya University, Kenya, with the approval number 4180. All procedures were conducted in accordance with the ethical standards of the institutional biosafety and laboratory guidelines.

Plants materials

Fresh leaves of *S. officinalis* were harvested during the dry season in Nyeri County, Kenya. The identification and authentication of the plant material was carried out at the Jomo Kenyatta University of Agriculture and Technology (JKUAT), Kenya, herbarium by a taxonomist and was assigned the voucher specimen number BC-JKUATBH/001.28/07/2025.

Pre-extraction and extraction procedures

The leaves were thoroughly rinsed with running tap water and subsequently air-dried under shade at room temperature (25°C) for 21 days. The dried leaves were ground into a fine powder using an electric blender (Model: IBL30U1, Itel, China) supplemented with a mortar and pestle to ensure uniform particle size. The powdered leaves were stored in an air-tight, light-resistant container until extraction. For extraction, 50 g of powdered leaves was soaked in 1 L of methanol in a conical flask and macerated with continuous shaking in a shaker incubator (GYROMAXTM 727, United States) at 140 rpm and room temperature (25°C) for 72 hours. Following extraction, the mixture was sequentially filtered through sieve cloth and Whatman Number 1 filter paper (Sterilin, Teddington, Middlesex, England) to remove particulate matter. The filtrate was concentrated on a rotary evaporator (Labtech DAIHAN, VP30, EV11, South Korea) at 65°C, 175 mbar reduced pressure, and 120 rpm. The resulting semi-solid extract was further dried in a hot-air oven at 37°C for 24 hours to a constant weight. The percentage yield of the crude extract was calculated and recorded as 10.17%, using Formula 1. Finally, the dried extract was stored in sterile Falcon tubes at 4°C until further use.

$$\text{Percentage (\%) yield} = \frac{Weight\ of\ the\ dried\ extract\ (g)}{Initial\ weight\ of\ the\ dried\ plant\ material\ (g)} \times 100 \qquad \text{(Formula 1)}$$

Phytochemical screening

Qualitative phytochemical screening procedures for different classes of secondary metabolites of the crude extract were conducted using established procedures employed by Yahaya et al. (2020), Noumi et al. (2023), and Rao et al. (2023) to analyze terpenoids, flavonoids, saponins, alkaloids, tannins, and phenols.

Terpenoids

Approximately 0.5 g of the crude extract was dissolved in 2 mL of chloroform (Sisco Research Laboratories Pvt. Ltd, India). Concentrated sulfuric acid (Loba Chemie Pvt. Ltd, India) was then carefully introduced along the wall of the test tube to form a distinct lower layer. The reddish-brown appearance was interpreted as evidence of terpenoid compounds.

Flavonoids

Approximately 0.5 g of the extract was reacted with small fragments of magnesium ribbon (FINAR Ltd, India), followed by gradual addition of concentrated hydrochloric acid (Finar Ltd, India). After five minutes of incubation, the appearance of a pink-to-magenta color indicated the presence of flavonoids.

Saponins

About 0.5 g of the extract was mixed with 2 mL of distilled water in a test tube and shaken vigorously. The formation and persistence of froth for about 10 minutes was indicative of saponins.

Alkaloids

Approximately 0.5 g of the extract was dissolved in dilute HCl (Finar Ltd, India) and filtered to obtain a clear solution. Wagner's reagent (Sigma-Aldrich, Germany) was then added to the filtrate solution, and the formation of a brownish or reddish precipitate confirmed the presence of alkaloids.

Tannins

About 0.5 g of the extract was heated with 10 mL of water and subsequently filtered. A few drops of 0.1% ferric chloride solution (Sisco Research Laboratories Pvt. Ltd, India) were added to the filtrate, and the appearance of blue-black or green-black color was interpreted as a positive result for tannins.

Phenols

About 3-4 drops of ferric chloride solution were added to 0.5 g of the extract. The appearance of a bluish-black color indicated the presence of phenolic compounds.

Gas chromatography mass-spectrometry

The chemical composition of the crude extract was analyzed using gas chromatography-mass spectrometry (GC-MS), following the procedure previously described by Konappa et al. (2020). The analysis was performed using a GC-MS system (Shimadzu GCMS-QP2010 SE, Japan) equipped with a low polarity BPX5 capillary column (30 m × 0.25 mm internal diameter, 0.25 µm film thickness). High-purity helium gas (99.99%) served as the carrier gas and was maintained at a constant flow rate of 1 mL/min. Ionization was carried out using the electron impact (EI) mode at 70 eV, with a scan interval of 0.2 seconds over a mass range of 40-600 m/z. A 1 µL sample volume was injected into the system, with the injector temperature set to 250°C. The column oven temperature program was initiated at 50°C and held for two minutes, then increased at 10°C/min to 200°C. The temperature was then raised to 280°C and maintained for 3 min to ensure complete elution of the compounds. Identification of the phytochemical components was accomplished by comparing the obtained mass spectra and chromatographic parameters, including retention times and peak features, with those of standard reference compounds available in the National Institute of Standards and Technology (NIST) spectral database.

Nanoencapsulation of *Salvia officinalis*

Sage-chitosan NPs were synthesized using an ionic gelation technique, according to the method reported by Portia et al. (2024). A 2% (w/v) chitosan was dissolved in 1% (v/v) aqueous acetic acid (Loba Chemie Pvt. Ltd, India) to obtain a 2% (w/v) polymer solution. The pH of the solution was subsequently adjusted to 4.8 using 1 N sodium hydroxide to optimize solubility. The resulting mixture was maintained under continuous magnetic stirring at 25°C for 24 hours for complete dissolution and homogeneity of the polymeric solution. A 40 mL portion of the chitosan solution was then mixed with Tween 80 (Griffchem, India) as a surfactant and stirred at 45°C for two hours to achieve a uniform solution. Methanolic extract of *S. officinalis* was added gradually at different weights (0, 0.2, 0.4, 0.6, 0.8, and 1 g) and stirred at 45°C for 30 minutes. Subsequently, 0.5% (w/v) tripolyphosphate (Griffchem, India) was added dropwise to the mixture under continuous stirring for 40 minutes to facilitate nanoparticle formation. The formed NPs were then recovered by centrifugation (ThermoFisher, Germany) at 4000 rpm for 30 minutes at 25°C, then washed several times with distilled water to remove unbound materials and excess reagent. To obtain a suspension, the NPs pellet was re-dispersed in 30 mL of distilled water after purification. The dispersion was then subjected to probe sonication using a probe sonicator (ThermoFisher, Germany) in an ice bath for four minutes at a pulsed cycle (2 seconds on, 1 second off) to enhance the uniformity. The resulting suspension was subsequently lyophilized at -65°C for 72 hours. The freeze-dried samples were collected in a sterile Falcon tube and stored at 4°C until further use.

Characterization of nanoparticles

The physicochemical properties of NPs, including size, shape, surface morphology, and surface functional groups, significantly influence their toxicity and biological activity (Samadian et al., 2020). Characterization of the NPs was carried out according to the methods described by Alkhathlan et al. (2020) and Daoudi et al. (2024). The optimal properties of the biosynthesized chitosan-sage NPs were evaluated using a UV-1800 UV-Visible spectrophotometer (Shimadzu, Kyoto, Japan) at a wavelength range of 200-700 nm using quartz cuvettes. Fourier transform infrared spectroscopy (FTIR) was conducted using the compact FTIR spectrometer ALPHA II (Bruker, Germany) over the spectral range of 4000-400 cm^{-1}. The FTIR analysis was performed to identify the functional groups present and to examine possible interactions between chitosan and the encapsulated phytocomponents. Surface morphology and structural characteristics were examined using scanning electron microscopy (SEM; JEOL 0860 0000 ALS [257], Japan), with a high accelerating voltage of 15 kV to obtain high-resolution images for detailed analysis.

Test organisms

The standard bacterial isolate of MRSA (ATCC 12493) and the clinical isolate of *A. baumannii* were obtained from Kenyatta University Referral Hospital, Nairobi, Kenya.

Determination of antimicrobial activity of biosynthesized chitosan-sage nanoparticles

Agar well diffusion method

Antimicrobial activity was evaluated using an agar well diffusion method as described by Enan et al. (2021) and Amou et al. (2025). Each Mueller-Hinton agar (MHA) plate (Oxoid Limited, United Kingdom) had six wells, representing different concentrations of the test sample and a negative control. Each Petri dish received 20 mL of sterile MHA, and evenly spaced wells (6 mm in diameter) were created around the margins using a sterilized cork borer. A Bunsen burner flame was employed during the process to ensure sterility. The bacterial test cultures were grown overnight in Mueller-Hinton broth and adjusted to a 0.5 McFarland standard using normal saline. A sterile cotton was immersed in the inoculum, excess liquid was gently drained, and the cotton was used to evenly inoculate the agar surface, which was then allowed to dry for 20 minutes. Aliquots (100 µL) of chitosan-sage NPs at concentrations of 500 µg/mL, 250 µg/mL, 125 µg/mL, 62.5 µg/mL, and 31.25 µg/mL were added into the wells. At the center of the plates, vancomycin and meropenem antibiotic discs were placed as positive controls for MRSA and *A. baumannii*, respectively (Saka et al., 2024). Each test was performed in triplicate and incubated at 37˚C for 18-24 hours. Zones of inhibition were measured using a ruler, and the three distinct readings from each plate were documented and analyzed to determine the mean and standard deviation (SD).

Minimum inhibitory concentration

In three replicates, 100 µL of Mueller-Hinton broth was dispensed into 96-well plates (Sterilin, Teddington, Middlesex, England), and 100 µL of each nano-formulated *S. officinalis* extract, the crude extract, and the positive controls were added in different wells of the first column of plates and serially diluted across the plates to obtain concentrations of 500, 250, 125, 62.5, and 31.25µg/mL. Then, 20 µL of the bacterial inoculum was added to all wells except those in the last column, which contained only broth to check sterility. Chitosan (2% w/v) and methanol were included as negative controls, whilst vancomycin and meropenem were employed as reference antibiotics for MRSA and *A. baumannii*, respectively. Following incubation at 37˚C for 18 hours, 20 µL of resazurin indicator (Glentham Life Sciences, United Kingdom) was added to each well, and the plates were further incubated at 37˚C for two hours. The minimum inhibitory concentration (MIC) was defined as the lowest concentration of the test sample that inhibited visible bacterial growth, as evidenced by the persistence of the blue color of the resazurin indicator, similar to the negative control.

Minimum bactericidal concentration

According to Mah (2014), the minimum bactericidal concentration (MBC) was the lowest concentration of an antimicrobial agent required to reduce the initial bacterial population by 99.9% or higher, after 18 to 24 hours of incubation at 37˚C. After incubation at 37˚C for 18 hours, test samples from wells containing concentrations exceeding the MIC were aseptically streaked onto MHA plates (using a sterile wire loop) and evaluated. The samples with the minimal concentration and no bacterial growth during incubation were indicated as MBC.

***In silico* analysis**

Bioactive compounds of the methanolic extract of *S. officinalis* with antimicrobial potential, identified by GC-MS analysis, were selected as ligands. Their 2D structures were retrieved from the PubChem database. Three-dimensional structures of the target proteins, namely the crystal structure of penicillin-binding protein 2a (PBP2a) double clinical mutant N146K-E150K from MRSA (ID: 4CPK) and the crystal structure of *A. baumannii* carbapenem-associated outer membrane protein (CarO; ID: 4FUV), were retrieved from the Research Collaboratory for Structural Bioinformatics

(RCSB) Protein Data Bank (PDB) in PDB format. The canonical SMILES representations of selected bioactive compounds were obtained and used as input ligands for docking analysis. Both protein and ligand files were prepared using appropriate preprocessing steps, including the removal of co-crystallized water molecules and conversion to Protein Data Bank charge type (Pdbqt) format. The ligand structures were energy-minimized before docking. Molecular docking simulations were conducted using AutoDock Vina (version 1.2.0) to predict the best binding pose and binding affinities (Bugnon et al., 2024). The binding regions were defined by setting a grid box with dimensions of 20 × 20 × 20 Å, centered on the active site using appropriate XYZ coordinates, and an exhaustiveness value of 4 was applied to control the search efficiency. The resulting complexes were visualized using BIOVIA Discovery Studio 2025 client software. Binding energies less than 0 indicated favorable interactions, with lower energy values suggesting stronger binding affinity (Khan and Lee, 2022).

Statistical analysis

All experiments were conducted in triplicate, and the present results were expressed as mean ± standard deviation (SD). Statistical and FTIR data analyses were performed using Origin Pro Lab 2026 (Student Version) software.

RESULTS

Phytochemical screening

The qualitative phytochemical analysis of the methanolic crude extract of *S. officinalis* indicated a high abundance of phenols, tannins, alkaloids, and saponins, while flavonoids and terpenoids were detected in moderate amounts (Table 1).

Gas chromatography-mass spectrometry

The mass spectrometer identified the nature and structural properties of chemical compounds by analyzing eluted samples at distinct time points. Peaks corresponding to the retention times of the compounds were observed in the chromatogram (Figure 1). The GC-MS of the methanolic crude extract of *S. officinalis* revealed compounds belonging to hydrocarbons, ketones, esters, cyclic compounds, and fatty acids classes, expressed as percentage area (Area%; Table 2).

Table 1. Qualitative phytochemical screening of *Salvia officinalis* crude extracts

Secondary metabolites	Methanolic crude extract of *Salvia officinalis*
Phenols	+++
Flavonoids	++
Tannins	+++
Alkaloids	+++
Terpenoids	++
Saponins	+++

+++: Abundantly present, ++: Moderately present

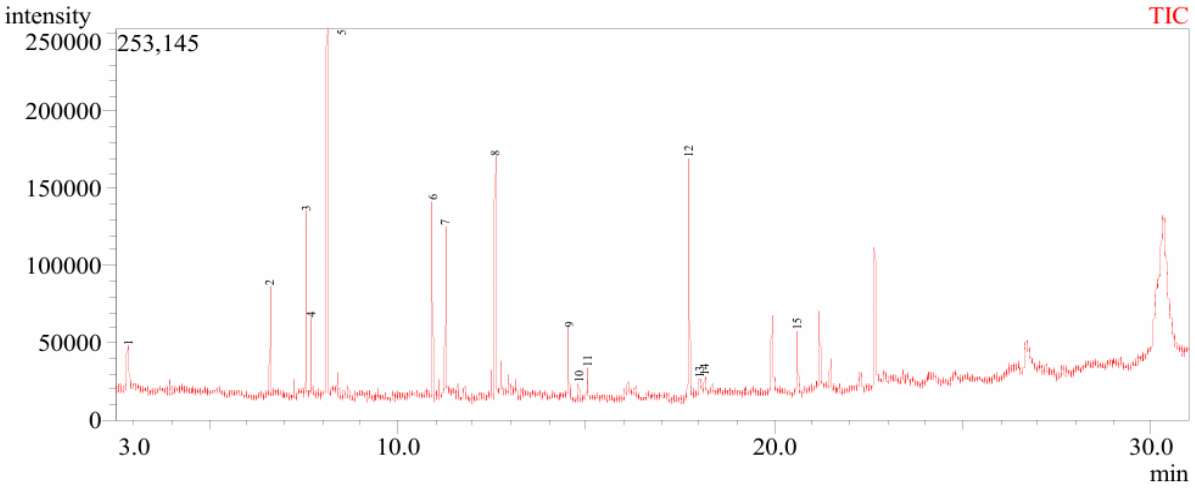

Figure 1. Gas chromatography-mass spectrometry of methanolic crude extract of *Salvia officinalis*

Table 2. Gas chromatography-mass spectroscopy analysis of methanolic crude extract of *Salvia officinalis*

Peaks	Retention time	Area (%)	Compounds names	Molecular weight (g/mol)	Molecular formula
1	2.839	4.87	2,2-Dimethoxybutane	118	$C_6H_{14}O_2$
2	6.595	4.71	Eucalyptol	154	$C_{10}H_{18}O$
3	7.558	7.93	Bicyclo[3.1.0]hexan-3-one,4-methyl-1-(1-methylethyl)	152	$C_{10}H_{16}O$
4	7.692	3.32	Thujone	152	$C_{10}H_{16}O$
5	8.116	16.56	Camphor	152	$C_{10}H_{16}O$
6	10.913	9.28	Caryophyllene	204	$C_{15}H_{24}$
7	11.263	7.66	1,4,7,-Cycloundecatriene, 1,5,9,9-tetramethyl-, Z,Z,Z-	204	$C_{15}H_{24}$
8	12.593	12.76	H-Cycloprop[e]azulene, decahydro-1,1,7-trimethyl-4-methylene	204	$C_{15}H_{24}$
9	14.535	3.87	Neophytadiene	278	$C_{20}H_{38}$
10	14.808	0.81	Phytol, acetate	338	$C_{22}H_{42}O_2$
11	15.028	2.28	3,7,11,15-Tetramethyl-2-hexadecen-1-ol	296	$C_{20}H_{40}O$
12	17.730	18.36	Naphthalene, decahydro-1,1,4a-trimethyl-6-methylene-5-(3-methyl-2,4-pentadienyl)-,[4aS-(4a.alpha.,5.alpha.,8a.beta.)]-	272	$C_{20}H_{32}$
13	18.010	1.82	3,7,11,15-Tetramethyl-2-hexadecen-1-ol	296	$C_{20}H_{40}O$
14	18.146	1.04	Humulane-1,6-dien-3-ol	222	$C_{15}H_{26}O$
15	20.598	4.75	4,5,6,7-Tetrahydroxy-1,8,8,9-tetramethyl-8,9-dihydrophenaleno[1,2-b]furan-3-one	342	$C_{19}H_{18}O_6$

Characterization of nanoparticles

Figure 2 exhibited the UV-visible absorption profile of *S. officinalis* chitosan NPs. A distinct absorption band centered at approximately 290 nm was observed in the spectrum, indicating the formation of the NPs. The FTIR analysis was employed to examine the chemical characteristics of the samples over a wavenumber range of 400-4000 cm^{-1}, enabling the identification of functional groups and assessment of potential interactions within the formulation. The absorption bands observed for chitosan-sage NPs and the crude extract are presented in Figure 3 and Table 3. Prominent peaks were detected at 3421 cm^{-1} in the NPs and at 3435 cm^{-1} in the crude extract, both representing strong broad O–H and NH_2 stretching, denoting hydroxyl and amide groups. Additionally, a medium broad peak at 1651 cm^{-1} was attributed to C=O (carbonyl) stretching (amide I group), and a weak broad peak at 1564 cm^{-1} corresponded to N–H stretching (amide II group). The band observed at 1412 cm^{-1} was associated with C-H bending vibrations of alkyl groups, and the distinct peak at 1257 cm^{-1} might have been attributed to C-N stretching vibrations corresponding to the amide III group. The prominent peak at 1125 cm^{-1} was indicative of P=O stretching vibrations, suggesting the presence of phosphate, while the absorption at 1024 cm^{-1} was assigned to C-O stretching vibrations of alcoholic groups. In the lower-wavenumber region, the band at 746 cm-1 might be related to C-Cl stretching in halogenated compounds, whereas the peak at 483 cm-1 was attributed to metal-oxygen (M-O) vibrations, indicating the presence of inorganic components.

The morphological features of the synthesized NPs were examined using SEM. The micrographs of the synthesized *S. officinalis* chitosan NPs demonstrated predominantly spherical particles with a relatively uniform distribution (Figure 4). Further analysis using ImageJ revealed that most of the NPs were in the 40-80 nm size range.

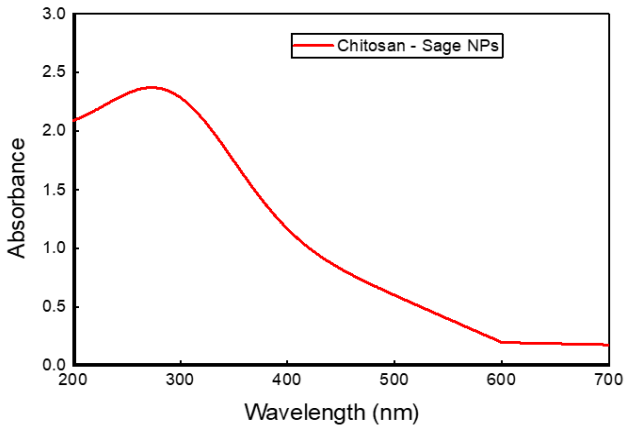

Figure 2. UV-Visible spectrum of biosynthesized chitosan-sage nanoparticles

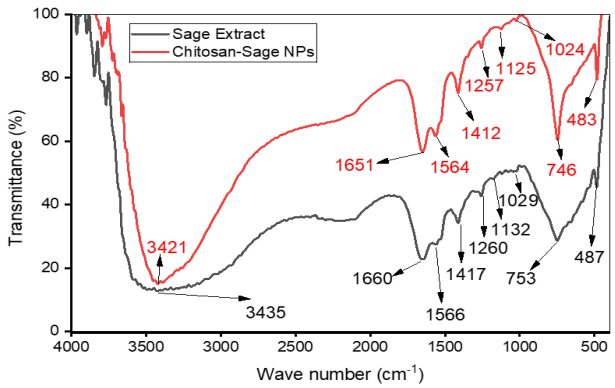

Figure 3. Fourier transform infrared spectra of biosynthesized chitosan-sage nanoparticles and sage crude extract

Table 3. Fourier transform infrared spectra of the functional group in chitosan-sage nanoparticles

Peak (cm^{-1})	Functional group
3421	O-H and NH_2 stretching / Hydroxyl and amide groups
1651	C=O Stretching / Amide I group
1564	N-H bending / Amide II group
1412	C-H bending / Alkyl group
1257	C-N stretching / Amide III group
1125	P=O stretching / Phosphate group
1024	C-O stretching / Alcoholic group
746	C-Cl stretching / Halo compound
483	M-O stretching / Metal-oxygen (Inorganic)

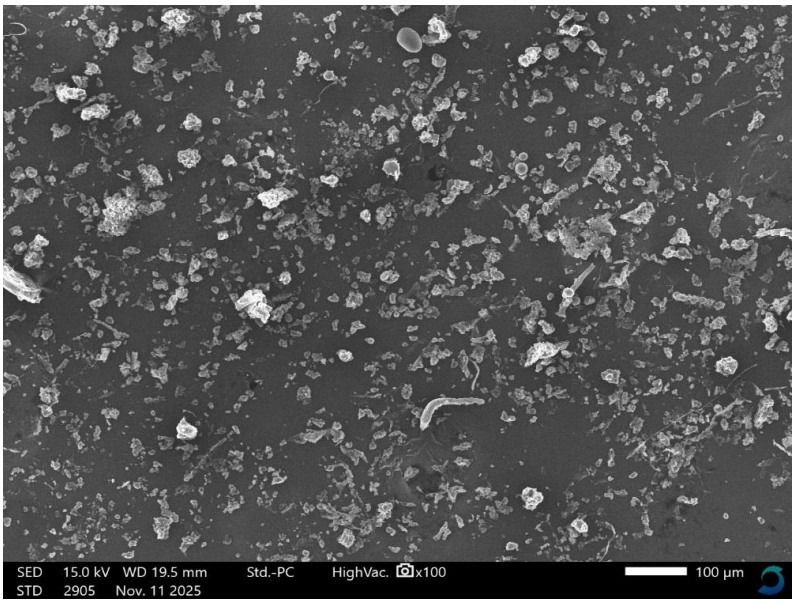

Figure 4. Scanning electron microscopy micrograph of biosynthesized chitosan-sage nanoparticle at 100x magnification

Antimicrobial activity of biosynthesized chitosan-sage nanoparticles

The antimicrobial potential of the biosynthesized *S. officinalis* chitosan NPs was evaluated using the agar well diffusion method (Table 4). The nano formulation demonstrated inhibitory effects against MRSA and *A. baumannii* across the tested concentrations, with greater inhibition observed at 500 µg/mL. At this concentration (500 µg/mL), clear zones of inhibition were recorded against MRSA and *A. baumannii,* indicating effective suppression of bacterial growth.

Minimum inhibitory concentration

The lowest concentrations required to prevent visible microbial growth were identified through MIC determination of chitosan-sage NPs. The NPs exhibited inhibitory activity at 62.5 µg/mL against MRSA and at 125 µg/mL against *A. baumannii*. In comparison, the MIC values for the crude extract were 250 and 500 µg/mL against MRSA and *A. baumannii,* respectively. Additionally, the positive controls had MICs of 25 µg/mL for vancomycin and 50 µg/mL for meropenem (Table 5).

Minimum bactericidal concentration

Chitosan-sage NPs inhibited the physical growth of MRSA at 125 µg/mL and *A. baumannii* at 500 µg/mL. The MBCs for the positive controls were 50 µg/mL for vancomycin and 100 µg/mL for meropenem (Table 6).

Table 4. Inhibition zones of chitosan-sage nanoparticles against methicillin-resistant *Staphylococcus aureus* and *Acinetobacter baumannii* following CLSI protocols

Bacterial organisms	*Salvia officinalis* nanoparticles (µg/mL)					Positive control	Negative control
	500	250	125	62.5	31.25	Vancomycin / meropenem	Methanol / normal saline
MRSA	21 ± 0.5	15 ± 1.0	12 ± 0.5	10 ± 0.5	0	17 ± 1.5	0
Acinetobacter baumannii	17 ± 1.5	13 ± 0.5	11 ± 1.0	9 ± 1.0	0	10 ± 1.5	0

CLSI: Clinical and laboratory standards institute, MRSA: Methicillin-resistant *Staphylococcus aureus*, NPs: Nanoparticles

To cite this paper: Chorr B, Kimotho J, and Kangogo M (2026). Antimicrobial Activity of Nano-encapsulated *Salvia Officinalis* against Methicillin-Resistant *Staphylococcus aureus* and *Acinetobacter Baumannii*. *World Vet. J.,* 16(2): 418-435. DOI: https://dx.doi.org/10.54203/scil.2026.wvj40

Table 5. Minimum inhibitory concentration of biosynthesized chitosan-sage nanoparticles

Bacterial organisms	*Salvia officinalis* nanoparticles (µg/mL)	Crude extract (µg/mL)	Standards antibiotics (µg/mL)	Negative controls (µg/mL)	
				Methanol	Chitosan
MRSA ATCC 12493	62.5	250	Vancomycin 25	Growth	Growth
Acinetobacter baumannii	125	500	Meropenem 50	Growth	Growth

MRSA: Methicillin-resistant *Staphylococcus aureus*

Table 6. Minimum bactericidal concentration of biosynthesized chitosan-sage nanoparticles

Bacterial organisms	*Salvia officinalis* nanoparticles (µg/mL)	Standards antibiotics (µg/mL)
MRSA	125	Vancomycin 50
Acinetobacter baumannii	500	Meropenem 100

MRSA: Methicillin-resistant *Staphylococcus aureus*

Molecular docking

The GC-MS analysis of the methanolic crude extract of *S. officinalis* identified a total of 15 bioactive compounds (Table 2). The phytochemical compounds were subsequently evaluated for their potential activity against MRSA and *A. baumannii* as demonstrated in Table 7. Molecular docking simulations were performed using AutoDock Vina (version 1.2.0) to assess their binding affinities toward the target proteins. Caryophyllene exhibited the strongest binding affinity with values of -6.7 kcal/mol for PBP2a and -6.3 kcal/mol for CarO. The interactions with both targets were mostly hydrophobic. The decahydro-naphthalene derivative exhibited a binding affinity of -6.6 kcal/mol for PBP2a and -6.3 kcal/mol for CarO, closely following caryophyllene. The interactions with PBP2a involved hydrogen bonding, hydrophobic contacts, and ionic interactions, whereas those with CarO involved hydrogen and hydrophobic bondings. Thujone demonstrated similar binding affinities, with scores of -5.7 kcal/mol for PBP2a and -5.8 kcal/mol for CarO. Thujone's interactions with both targets included hydrogen bonding and hydrophobic interactions. Camphor exhibited binding affinities of -5.7 kcal/mol for PBP2a (via hydrogen bonds and hydrophobic interactions) and -5.5 kcal/mol for CarO (through hydrophobic interactions). Eucalyptol exhibited a binding affinity of -5.6 kcal/mol for PBP2a, including hydrogen bonding and hydrophobic interactions, and a relatively lesser affinity of -4.9 kcal/mol for CarO via hydrogen bonding. Neophytadiene had moderate affinities of -5.6 kcal/mol for PBP2a and -5.0 kcal/mol for CarO.

Table 7. Molecular docking of phytocompounds against methicillin-resistant *Staphylococcus* and *Acinetobacter baumannii*

Phytocompounds	Binding affinity (Kcal/mol)		Interactions	
	PBP2a (4CPK) MRSA	CarO (4FUV) *A. baumannii*	PBP2a (4CPK) MRSA	CarO (4FUV) *A. baumannii*
Eucalyptol	-5.6	-4.9	H-bond, Hydrophobic	H-bond
Thujone	-5.7	-5.8	H-bond, Hydrophobic	H-bond, Hydrophobic
Camphor	-5.7	-5.5	H-bonds, Hydrophobic	Hydrophobic
Caryophyllene	-6.7	-6.3	Hydrophobic	Hydrophobic
Neophytadiene	-5.6	-5.0	Hydrophobic	Hydrophobic
Naphthalene, decahydro-1,1,4a-trimethyl-6-methylene-5-(3-methyl-2,4-pentadienyl)	-6.6	-6.3	H-bond, Hydrophobic, and ionic interactions	H-bond, Hydrophobic

PBP2a: Penicillin binding protein 2a, CarO: Carbapenem-associated outer membrane protein, MRSA: Methicillin-resistant *Staphylococcus aureus, A. baumannii: Acinetobacter baumannii*

A

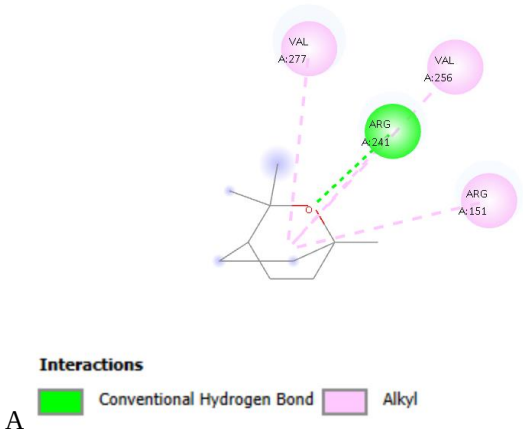
VAL
A:277
VAL
A:256
ARG
A:241
ARG
A:151
Interactions
Conventional Hydrogen Bond
Alkyl

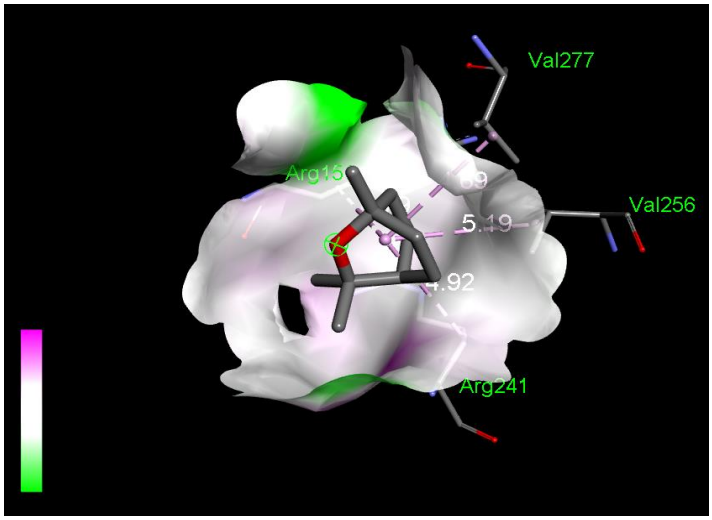
Val277
Arg151
5.19
Val256
4.92
Arg241

B

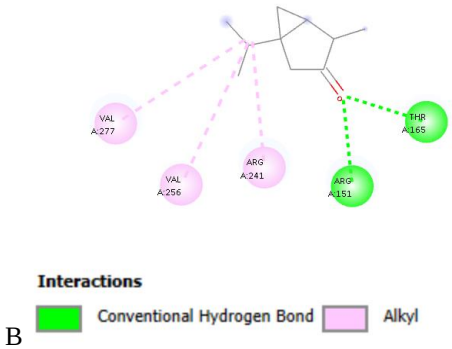
VAL
A:277
VAL
A:256
ARG
A:241
ARG
A:151
THR
A:165
Interactions
Conventional Hydrogen Bond
Alkyl

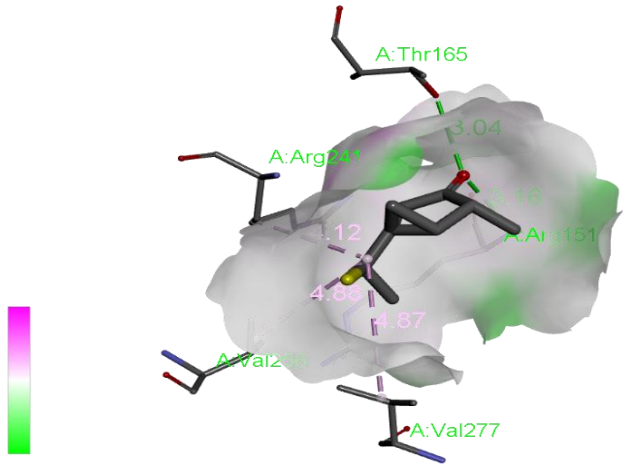
A:Thr165
3.04
A:Arg241
4.12
4.87
A:Val277

C

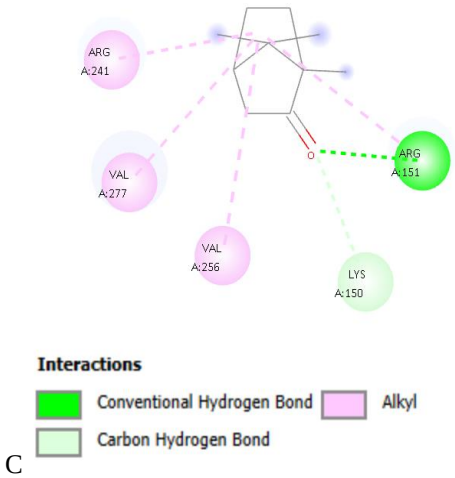
ARG
A:241
VAL
A:277
VAL
A:256
ARG
A:151
LYS
A:150
Interactions
Conventional Hydrogen Bond
Alkyl
Carbon Hydrogen Bond

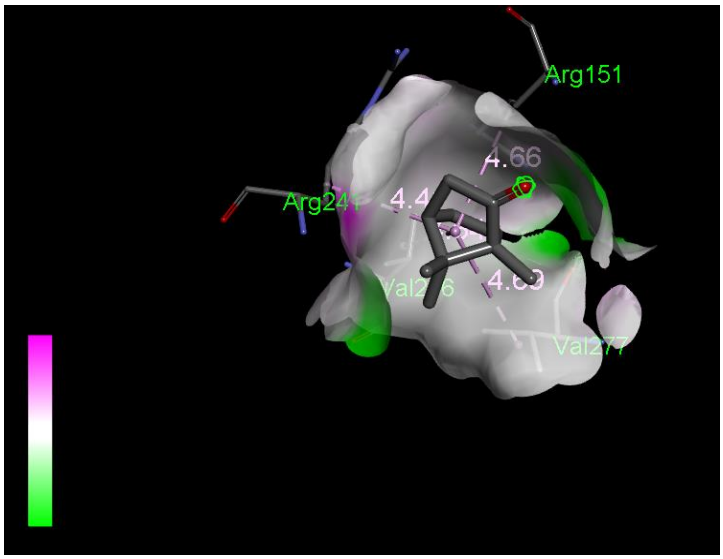
Arg151
4.66
Arg241
4.4
Val277

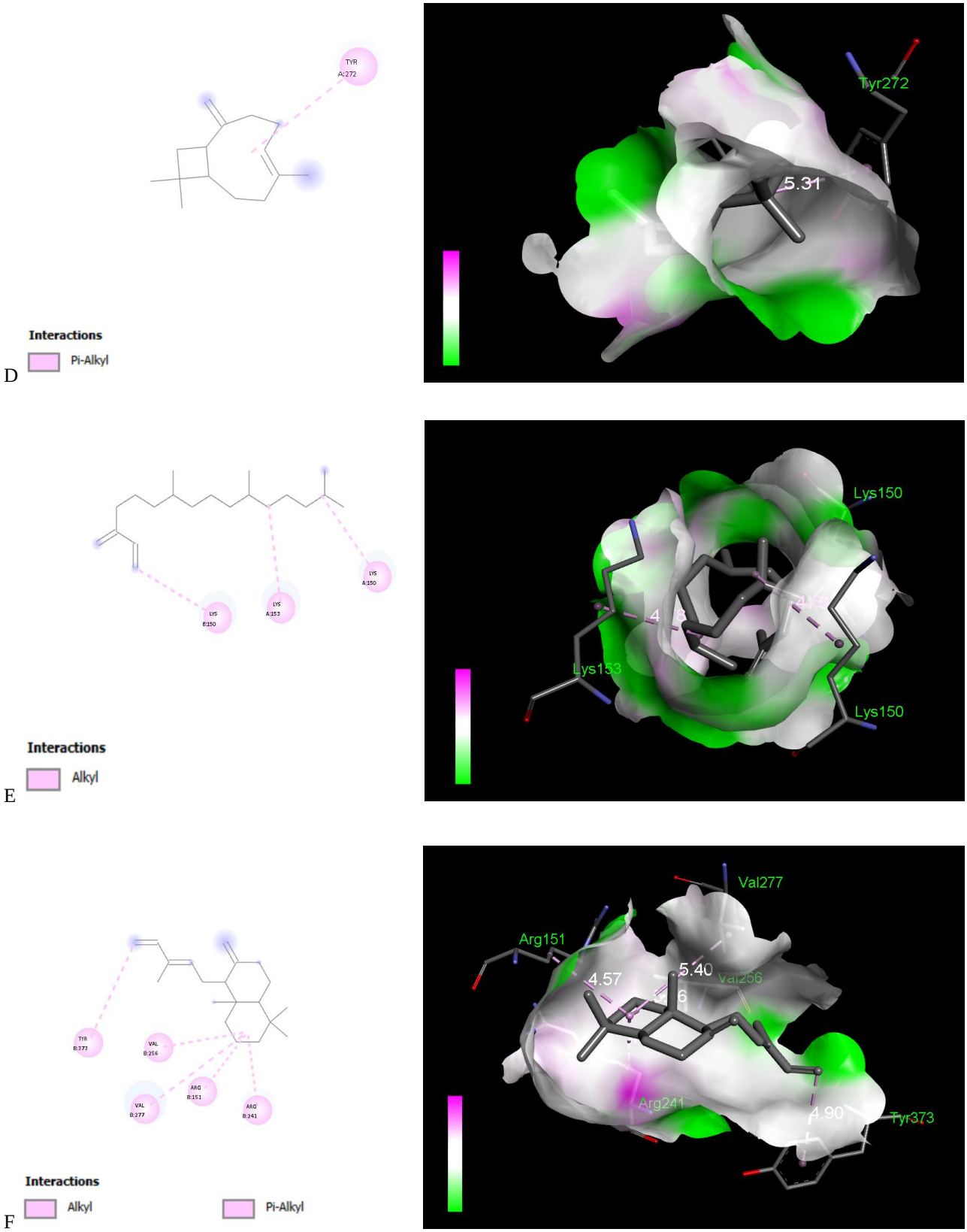

Figure 5. The 2D diagrams and 3D interaction profiles illustrating ligand binding for six compounds within the binding site of PBP2a. **Å:** Interaction distances, **A:** Eucalyptol, **B:** Thujone, **C:** Camphor, **D:** Caryophyllene, **E:** Neophytadiene, **F:** Naphthalene.

A

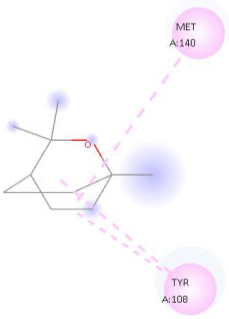
MET
A:140
TYR
A:108


Interactions
Alkyl
Pi-Alkyl

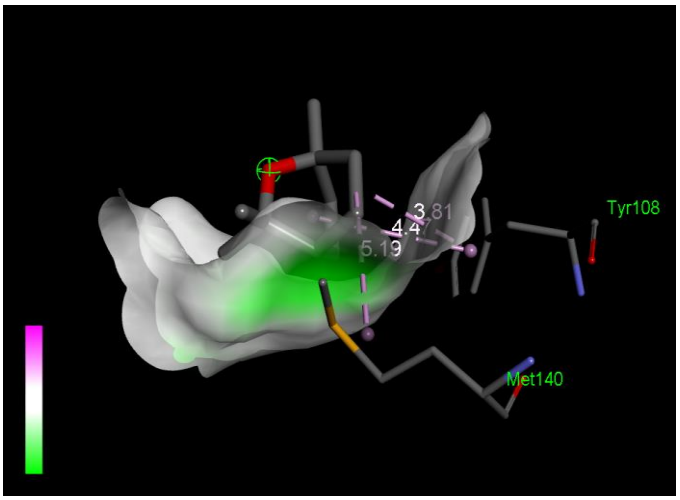
3.81
4.4
5.19
Tyr108
Met140

B

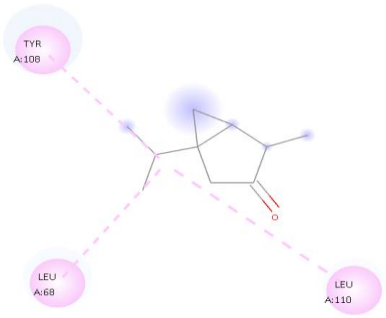
TYR
A:108
LEU
A:68
LEU
A:110


Interactions
Alkyl
Pi-Alkyl

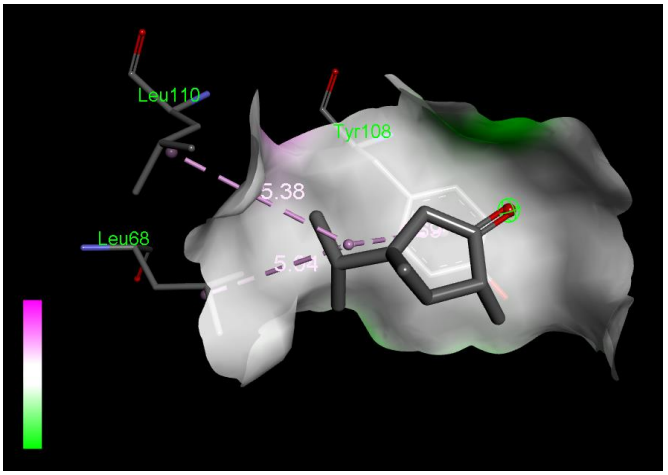
Leu110
Tyr108
5.38
Leu68

C

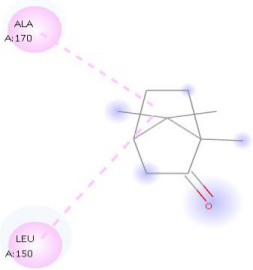
ALA
A:170
LEU
A:150


Interactions
Alkyl

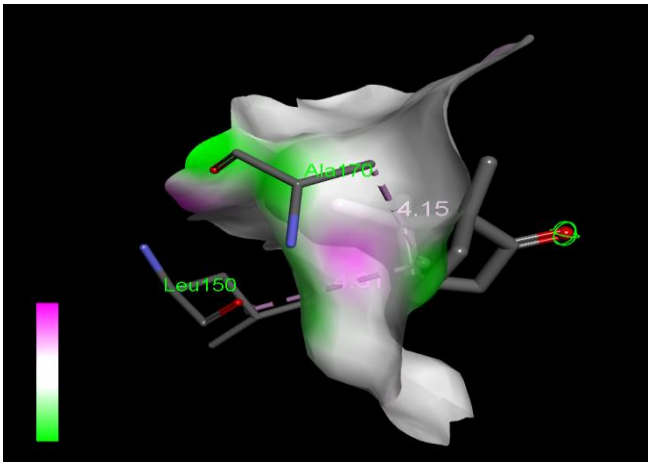
4.15
Leu150

D

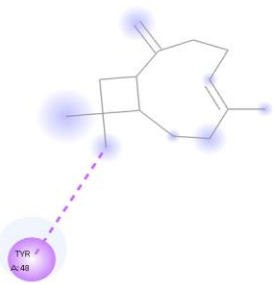
TYR
A:48


Interactions
Pi-Sigma

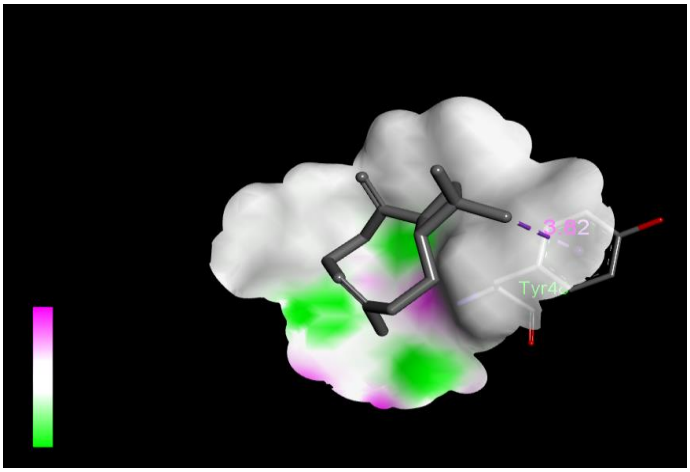

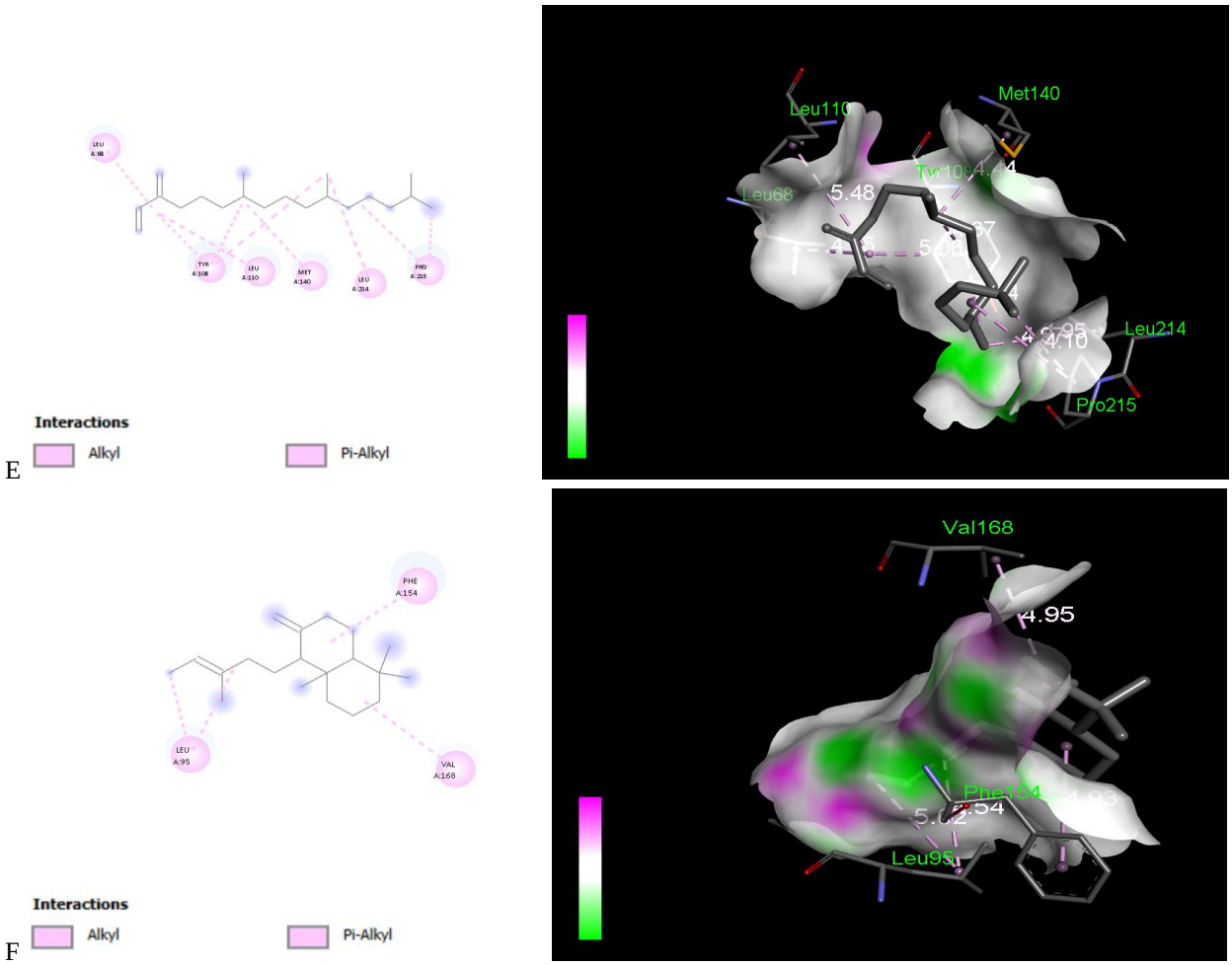

Figure 6. The 2D diagrams and 3D interaction profiles illustrating ligand binding for six compounds within the binding site of CarO. **Å:** Interaction distances, **A:** Eucalyptol, **B:** Thujone, **C:** Camphor, **D:** Caryophyllene, **E:** Neophytadiene, **F:** Naphthalene.

DISCUSSION

The qualitative phytochemical screening of *S. officinalis* crude methanolic extract revealed the presence of bioactive secondary metabolites, including phenols, flavonoids, tannins, alkaloids, terpenoids, and saponins. Such secondary metabolites are responsible for the medicinal activity of plants (Kumari et al., 2017). The presence of these metabolites may explain the observed antimicrobial activity and support the plant's traditional (folkloric) use in managing different diseases (Kanarek et al., 2025). This finding aligned with those of Khadse (2019) and Patel et al. (2024), who reported similar phytochemical profiles in *S. officinalis* leaf extract. The high concentration of these compounds' likely accounts for their potent antimicrobial activity, which was consistent with the findings of Amal and Wael (2016), who demonstrated that the biologically active polyphenolic components in *S. officinalis* extracts exhibit significant antimicrobial activity.

The GC-MS analysis of the *S. officinalis* methanolic extract revealed 15 peaks, representing the presence of 15 different compounds. The most abundant components included naphthalene (peak 12, 18.36%), camphor, thujone, eucalyptol, and neophytadiene. Previous studies have reported the antimicrobial properties of these compounds (Selim et al., 2022; He et al., 2026), further supporting the antimicrobial potential of *S. officinalis*. The existence of bioactive compounds supported the traditional medicinal applications of *S. officinalis* (Anjali et al., 2024).

The UV-visible spectroscopy was employed as a preliminary technique to confirm the NPs formation. The biosynthesized chitosan-sage NPs were analyzed across a wavelength range of 200-700 nm. A maximum absorbance peak was observed at 290 nm, which was consistent with previous reports on plant-mediated nano-formulations, where absorption bands in the range of 270-320 nm were typically attributed to phenolic-rich extracts and their involvement in NPs interaction or stabilization (Kolahalam et al., 2019; Jamzad and Kamari Bidkorpeh, 2020). These findings were similar to those of El-Naggar et al. (2022), who reported an absorbance peak at 295 nm, while El-Naggar et al. (2024) observed a peak at 285 nm for the chitosan standard. Furthermore, Dutta et al. (2023) reported an absorbance band for chitosan NPs at 330.25 nm.

FTIR analysis characterized the functional groups present in the biosynthesized chitosan NPs derived from *S. officinalis* leaf extracts. The FTIR technique provided insight into the interactions between chitosan and phytochemicals within the extract. Typical functional groups in chitosan NPs include amide (-NH_2), hydroxyl (-OH), and C–H, C–N, C–O, and P=O bonds (Boruah and Dutta, 2021). The broad absorption band observed between 3000 and 3500 cm^{-1}, corresponding to (-OH) and (-NH_2) groups, was considered a key indicator of the chitosan NPs formation (Parida et al., 2013). The present study recorded a peak at 3421 cm^{-1}, aligning with the findings of Krishnaveni and Ragunathan (2015), who observed a band at 3437 cm^{-1} in a chitosan standard sample attributed to strong dimeric O–H stretching. Similarly, Choudhary et al. (2017) reported a peak at 3424 cm^{-1} associated with a combined amide (-NH_2) and hydroxyl (-OH) groups. The peak at 1651 cm^{-1} was attributed to C=O stretching vibrations of the amide carbonyl group (Zhang et al., 2017). The band observed at 1564 cm^{-1} indicated the presence of a primary amine group, associated with the N-H bending vibration. Although Sathiyabama et al. (2024) reported a C-H stretching peak at 2927 cm^{-1} as a chitosan structure indicator, the present study identified C–H bonds in chitosan-sage NPs at 1412 cm^{-1}. The peak at 1125 cm^{-1}, corresponding to P=O stretching, confirmed ionic cross-linking between tripolyphosphate and chitosan, which was essential for nanoparticle formation (López-León et al., 2005). Similarly, Boruah and Dutta (2021) reported the same functional groups at closely matching wavenumbers. The C-O stretching vibration of the glycosidic linkage appeared at 1024 cm^{-1} in the present study, which was close to the peak at 1029 cm^{-1} reported by Sathiyabama et al. (2024). Additionally, minor peaks at 746 cm^{-1} and 483 cm^{-1} corresponded to lower frequency skeletal bending of the chitosan backbone (Zhang et al., 2017).

The SEM analysis revealed that the biosynthesized *S. officinalis* chitosan NPs were relatively homogeneous, with particle size well-dispersed and spherical in shape. These findings were consistent with those of Sharma et al. (2013), who reported that chitosan NPs typically exhibit spherical morphology with smooth surfaces. In the present study, particle sizes ranged from 40 to 80 nm, which was comparable to the range of sizes of 33.64 and 74.87 nm reported by Khanmohammadi et al. (2015) using field emission SEM.

The antimicrobial evaluation of the biosynthesized chitosan-sage NPs demonstrated susceptibility in MRSA (Gram-positive) and *A. baumannii* (Gram-negative), with MRSA exhibiting greater sensitivity than the crude extract of *S. officinalis*. A study conducted by Randhawa et al. (2018) on the methanolic crude extract of *S. officinalis* against the standard reference strains of MRSA and *A. baumannii* revealed the sensitivity of these organisms. Previous studies revealed the antimicrobial efficacy of the crude extract of *S. officinalis*; however, these studies utilized non-encapsulated extracts, which could be constrained by poor stability, rapid degradation, and the reduced bioavailability of active compounds (Rudhani, 2018; Mendes et al., 2020; Al-Qaysi and Al-Tulaibawi, 2022). In contrast, the present study employed a chitosan-based nano-formulation, which offered several advantages, including enhanced stability, improved solubility, and controlled release of phytocomponents. Furthermore, nanoscale delivery systems can facilitate the interaction with microbial cell membranes, potentially increasing antimicrobial efficacy (Chandrasekaran et al., 2020). Therefore, the nano-encapsulation approach may offer improved antimicrobial efficacy compared to the conventional crude extract applications, suggesting its potential as a promising strategy for enhancing phytochemical delivery and antibacterial activity. Karagözlü and Özeşer (2024) reported that silver NPs synthesized from *S. officinalis* indicated inhibition zones measuring 10.5, 10, 9, and 7 mm against *Escherichia coli*, *Pseudomonas aeruginosa*, *S. aureus*, and *Bacillus subtilis*, respectively. The biosynthesized chitosan-sage NPs demonstrated maximum antimicrobial activity at 500 µg/mL, with inhibition zones reaching 21 mm for MRSA and 17 mm for *A. baumannii*. Furthermore, the MIC of chitosan-sage NPs against MRSA and *A. baumannii* was 62.5 µg/mL and 125 µg/mL, respectively, while the MBC was 125 µg/mL for MRSA and 500 µg/mL for *A. baumannii*. Lower MIC and MBC values indicated greater susceptibility of the microorganism to the tested antimicrobial agent (Balouiri et al., 2016). Therefore, MRSA was more susceptible to chitosan-sage NPs compared to *A. baumannii*. The reduced susceptibility observed in *A. baumannii* relative to MRSA might be due to the presence of an outer membrane in Gram-negative bacteria, a barrier that limited the entry of antimicrobial agents (Lazar et al., 2023). Nonetheless, the activity observed against *A. baumannii* and MRSA suggested a broad-spectrum effect of the nano-formulation. The absence of antimicrobial activity in the negative controls confirmed that the antibacterial activity was attributable to the formulated NPs rather than the solvent system. Nano-chitosan exhibited greater efficacy than its bulk chitosan due to its unique physico-chemical characteristics, which facilitated penetration through cell walls and membranes (Naskar et al., 2019). Chitosan NPs have been widely recognized for broad-spectrum antimicrobial properties (Ke et al., 2021; Dutta et al., 2023; Dou et al., 2024).

The increasing global threat of multidrug-resistant bacteria, particularly MRSA and carbapenem-resistant *A. baumannii*, underscored the urgent need for novel antimicrobial strategies (Kar et al., 2023; Mohamed et al., 2025). Molecular docking served as a computational approach for the preliminary screening and identification of potential key compounds from different sources, including natural phytocompounds, by predicting their binding affinities and interaction mechanisms with specific bacterial targets (Kar et al., 2021; Tabassum et al., 2023; Shalini et al., 2024).

Molecular docking enables the systematic development of novel therapies, particularly targeting notable resistance factors, such as PBP2a in MRSA porin and CarO in *A. baumannii* (Rosado et al., 2025; Swain and Pan, 2025). The PBP2a is a major target for the development of new anti-MRSA treatment agents, including allosteric modification and direct inhibition (Sanapalli et al., 2025). *Acinetobacter baumannii* presented a notable challenge owing to its extensive drug resistance and biofilm-forming capacity, and porins such as CarO further reinforce its resistance profile (Tram et al., 2021; Lokhande et al., 2023). The current study examined the molecular docking of certain phytocompounds, including eucalyptol, thujone, camphor, caryophyllene, neophytadiene, and a derivative of decahydro-naphthalene against PBP2a of MRSA and CarO of *A. baumannii*, to evaluate their potential as antimicrobial agents. The binding affinities observed at -4.9 to -6.7 kcal/mol indicated moderate to strong interactions, suggesting that these compounds may contribute to antibacterial activity by targeting essential bacterial proteins. Notably, compounds such as caryophyllene and the naphthalene derivative exhibited relatively higher binding affinities, suggesting a strong potential to disrupt protein function. Previous studies have highlighted caryophyllene's role in preventing biofilm formation in *S. aureus* and its presence in plant essential oils with antibacterial properties (Setiawansyah and Gemantari, 2022; Sharma et al., 2025). Additionally, camphor, thujone, eucalyptol, and neophytadiene exhibited moderate binding affinities closely following that of caryophyllene and the naphthalene derivative (Juzer et al., 2022; Vinutha et al., 2025). Neophytadiene has been identified from different plant extracts and studied for its inhibitory effects on biofilm formation in *S. aureus* (Maheswari and Kalaiselvi, 2024; Pouline et al., 2024). The slightly lowered affinity of eucalyptol and neophytadiene for CarO could be related to the fewer polar interactions, emphasizing the need for specific interaction types to achieve effective binding (Noumi et al., 2023; Khatoon et al., 2024).

The PBP2a is a critical enzyme responsible for β-lactam resistance in MRSA, and its inhibition can disrupt peptidoglycan crosslinking, ultimately compromising bacterial cell wall integrity (Shidiki and Vyas, 2022). The observed interactions, including hydrogen bonding and hydrophobic interactions, were consistent with previous studies demonstrating that stable ligand-protein interactions enhanced the inhibitory effect by improving binding stability in the active or allosteric sites (Verma et al., 2022). Similarly, interactions with the CarO protein, which was involved in membrane permeability in *A. baumannii*, suggested that eucalyptol, thujone, camphor, caryophyllene, neophytadiene, and naphthalene derivatives may interfere with nutrient transport or membrane-associated processes, thereby contributing to antibacterial effects.

The predominance of hydrophobic interactions observed for most of the compounds, particularly terpenoids, such as caryophyllene and neophytadiene, could be related to their nonpolar nature, which improved binding within the hydrophobic regions of target proteins. Moreover, the presence of hydrogen bonding in some compounds, including eucalyptol and thujone, may further stabilize ligand-protein complexes, enhancing biological activity. Importantly, the binding energies observed in the present study fell within the range reported for other bioactive phytochemicals with proven antimicrobial activity, supporting their possible role as key compounds (Degfie et al., 2022).

CONCLUSION

In the present study, chitosan NPs were biosynthesized using *S. officinalis* leaf extracts as part of a nanomedicine approach to address the growing challenge of AMR. The prepared NPs exhibited notable antimicrobial activity against multidrug-resistant MRSA and *A. baumannii* strains. The improved performance observed for the chitosan-based nano-formulation, compared to the crude extract, might be attributed to enhanced surface reactivity, improved dispersion, and more efficient interaction with microbial cells. The present findings indicated that such nanoscale systems could serve as viable candidates for antimicrobial applications. However, the present study was limited by the absence of absorption, distribution, metabolism, excretion, and toxicity (ADMET) analysis, *in vivo* evaluation, and cytotoxicity assessment, as well as the lack of detailed investigation into the long-term stability of the NPs under physiological conditions. Therefore, further studies are required to establish the safety, therapeutic efficacy, and stability of chitosan-sage NPs before potential clinical application.

DECLARATION

Acknowledgements

The authors sincerely acknowledged the support provided by the African Union through the Pan African University Institute for Basic Sciences, Technology, and Innovation, Kenya, in facilitating this study. The authors extend their appreciation to the Food Fortification and Chemistry Laboratories at Jomo Kenyatta University of Agriculture and Technology (JKUAT), Kenya, and the Kenya Medical Research Institute (KEMRI), for granting access to the facilities used in the present study.

Authors' contributions

Bakary Chorr conducted the laboratory experiments, data analysis, and drafted the original manuscript. James Kimotho and Mourine Kangogo supervised, reviewed, and edited the study. All authors have read and agreed to publish the final edition of the manuscript.

Availability of data and materials

The data generated during the present study are available from the corresponding author upon reasonable request.

Competing interests

The authors have declared no conflict of interest.

Ethical considerations

All authors have checked and confirmed ethical issues, including plagiarism, consent to publish, misconduct, data fabrication and/or falsification, double publication and/or submission, and redundancy. The authors have not used any AI tools for writing or preparing the present manuscript.

Funding

Funding was provided by the Pan African University Institute for Basic Science, Technology, and Innovation, Kenya.

REFRENCES

Ahmed SK, Hussein S, Qurbani K, Ibrahim RH, Fareeq A, Mahmood KA, and Mohamed MG (2024). Antimicrobial resistance: Impacts, challenges, and future prospects. Journal of Medicine, Surgery, and Public Health, 2: 100081. DOI: https://www.doi.org/10.1016/j.glmedi.2024.100081

Ali A, Basha O, and Ibrahim M (2017). Incidence of methicillin-resistant staphylococcus aureus isolation from sheep and goat. Alexandria Journal of Veterinary Sciences, 54(1): 142. DOI: https://www.doi.org/10.5455/ajvs.244291

Alkhathlan AH, AL-Abdulkarim HA, Khan M, AlDobiy A, Alkholief M, Alshamsan A, Alkhathlan HZ, and Siddiqui MRH (2020). Ecofriendly synthesis of silver nanoparticles using aqueous extracts of *Zingiber officinale* (Ginger) and *Nigella sativa* L. Seeds (*Black cumin*) and comparison of their antibacterial potential. Sustainability, 12(24): 10523. DOI: https://www.doi.org/10.3390/su122410523

Al-Qaysi DBA and Al-Tulaibawi NAJ (2022). Antibacterial efficacy of salvia officinalis extract against *Staphylococcus aureus* and *Escherichia Coli*. International Journal of Design and Nature and Ecodynamics, 17(5): 789-794. DOI: https://www.doi.org/10.18280/ijdne.170518

Amal M and Wael M (2016). Phytochemical and biochemical studies of sage (*Salvia officinalis* L.). Pharmaceutical and Biosciences Journal, 4(5): 56-62. DOI: https://www.doi.org/10.20510/ukjpb/4/i5/118037

Amou B, Ajayi TO, and Dada-Adegbola HO (2025). Antimicrobial activity of *Terminalia leiocarpa Baill*. and *Terminalia avicennioides Guill* and *Perr*. Root bark extracts in resistant clinical isolates. Journal of Pharmacy and Pharmacognosy Research, 13(2): 633-646. DOI: https://www.doi.org/10.56499/jppres24.2010_13.2.633

Balouiri M, Sadiki M, and Ibnsouda SK (2016). Methods for in vitro evaluating antimicrobial activity: A review. Journal of Pharmaceutical Analysis, 6(2): 71-79. DOI: https://www.10.1016/j.jpha.2015.11.005

Boruah S and Dutta P (2021). Fungus mediated biogenic synthesis and characterization of chitosan nanoparticles and its combine effect with *Trichoderma asperellum* against *Fusarium oxysporum, Sclerotium rolfsii* and *Rhizoctonia solani*. Indian Phytopathology, 74(1): 81-93. DOI: https://www.doi.org/10.1007/s42360-020-00289-w

Bugnon M, Röhrig UF, Goullieux M, Perez MAS, Daina A, Michielin O, and Zoete V (2024). SwissDock 2024: Major enhancements for small-molecule docking with Attracting Cavities and AutoDock Vina. Nucleic Acids Research, 52(W1): W324-W332. DOI: https://www.doi.org/10.1093/nar/gkae300

Castillo-Ramírez S, Aguilar-Vera A, Kumar A, and Evans B (2025). *Acinetobacter baumannii*: Much more than a human pathogen. Antimicrobial Agents and Chemotherapy, 69(9): e00801-25. DOI: https://www.doi.org/10.1128/aac.00801-25

Chandrasekaran M, Kim KD, and Chun SC (2020). Antibacterial activity of chitosan nanoparticles: A review. Processes, 8(9): 1173. DOI: https://www.doi.org/10.3390/pr8091173

Choudhary RC, Kumaraswamy RV, Kumari S, Pal A, Raliya R, Biswas P, and Saharan V (2017). Synthesis, characterization, and application of chitosan nanomaterials loaded with zinc and copper for plant growth and protection. Nanotechnology Springer., Singapore, pp. 227-247. DOI: https://www.doi.org/10.1007/978-981-10-4573-8_10

Daoudi H, Bouafia A, Laouini SE, Meneceur S, Fellah M, Iqbal A, El-Hiti GA, and Selmi B (2024). *In vitro* and *in silico* study of biosynthesized silver nanoparticles using *Nigella sativa* extract against SARS-CoV-2 and *Candida albicans*. Journal of Molecular Liquids, 405: 125059. DOI: https://www.doi.org/10.1016/j.molliq.2024.125059

Degfie T, Endale M, Tafese T, Dekebo A, and Shenkute K (2022). *In vitro* antibacterial, antioxidant activities, molecular docking, and ADMET analysis of phytochemicals from roots of Hydnora johannis. Applied Biological Chemistry, 65(1): 76. DOI: https://www.10.1186/s13765-022-00740-8

Devi R, Kumar N, Kurbah I, Kumar S, Nehta R, Sharma A, and Devi U (2026). Exploring the role of nanotechnology in medicinal plant systems: A pathway to improved growth and bioactive compound production. South African Journal of Botany, 189: 442-454. DOI: https://www.doi.org/10.1016/j.sajb.2025.12.005

Dewi MK, Chaerunisaa AY, Muhaimin M, and Joni IM (2022). Improved activity of herbal medicines through nanotechnology. Nanomaterials, 12(22): 4073. DOI: https://www.doi.org/10.3390/nano12224073

Dou X, Fan N, Yang J, Zhang Z, Wu B, Wei X, and Feng Y (2024). Research progress on chitosan and its derivatives in the fields of corrosion inhibition and antimicrobial activity. Environmental Science and Pollution Research, 31(21): 30353-30369. DOI: https://www.10.1007/s11356-024-33351-5

Dutta P, Kumari A, and Mahanta M (2023). Chitosan nanoparticle: Synthesis, characterization, and use as plant health materials. In: B. Kumar (Editor), Biochemistry. IntechOpen, chapter 4. DOI: https://www.doi.org/10.5772/intechopen.106502

El-Naggar NEA, Saber WIA, Zweil AM, and Bashir SI (2022). An innovative green synthesis approach of chitosan nanoparticles and their inhibitory activity against phytopathogenic *Botrytis cinerea* on strawberry leaves. Scientific Reports, 12(1): 3515. DOI: https://www.doi.org/10.1038/s41598-022-07073-y

El-Naggar NEA, Shiha AM, Mahrous H, and Mohammed ABA (2024). A sustainable green-approach for biofabrication of chitosan nanoparticles, optimization, characterization, its antifungal activity against phytopathogenic *Fusarium culmorum* and antitumor activity. Scientific Reports, 14(1): 11336. DOI: https://www.doi.org/10.1038/s41598-024-59702-3

Enan ET, Ashour AA, Basha S, Felemban NH, and Gad El-Rab SMF (2021). Antimicrobial activity of biosynthesized silver nanoparticles, amoxicillin, and glass-ionomer cement against *Streptococcus mutans* and *Staphylococcus aureus*. Nanotechnology, 32(21): 215101. DOI: https://www.doi.org/10.1088/1361-6528/abe577

Ezema CA, Aguchem RN, Aham EC, Ezeorba WFC, Okagu IU, and Ezeorba TPC (2024). *Salvia Africana-lutea L.*: A review of ethnobotany, phytochemistry, pharmacology applications and future prospects. Advances in Traditional Medicine, 24(3): 703-724. DOI: https://www.doi.org/10.1007/s13596-023-00726-x

Esfandiari AH, Mobarezi Z, Afarande H, Mahaki H, Ketabi K, Manoochehri H, Sheykhhasan M, Avan A, Meshkat Z, and Tanzadehpanah H (2025). Electrode modification in viral biosensors: A review. Current Medicinal Chemistry, 32(36): 8011-8034. DOI: https://www.doi.org/10.2174/0109298673358036250303025326

Ghorbani A and Esmaeilizadeh M (2017). Pharmacological properties of *Salvia officinalis* and its components. Journal of Traditional and Complementary Medicine, 7(4): 433-440. DOI: https://www.doi.org/10.1016/j.jtcme.2016.12.014

He Y, Wang Y, Hu H, Hu Y, Hua Q, Wu Y, Li D, and Liu Z (2026). Unraveling the antibacterial mechanism of eucalyptol against *Escherichia coli* O157:H7 through transcriptomics and its application in beef broth. International Journal of Food Microbiology, 448: 111580. DOI: https://www.doi.org/10.1016/j.ijfoodmicro.2025.111580

Jamzad M and Kamari Bidkorpeh M (2020). Green synthesis of iron oxide nanoparticles by the aqueous extract of Laurus nobilis L. leaves and evaluation of the antimicrobial activity. Journal of Nanostructure in Chemistry, 10(3): 193-201. DOI: https://www.10.1007/s40097-020-00341-1

Juzer T, Ranjani S, and Hemalatha S (2022). Camellia sinensis mediated synthesis and characterization of nanoparticles and applications to control Gram-negative ESBL producing antibiotic resistant bacterial pathogens. Food Bioscience, 50: 102070. DOI: https://www.doi.org/10.1016/j.fbio.2022.102070

Khadse PM (2019). Qualitative phytochemical analysis and pharmacological studies of Salvia officinalis. International Journal of Life Sciences, A13: 270-272. Available at: http://oaji.net/articles/2020/736-1579610617.pdf

Kanarek P, Breza-Boruta B, and Stocki M (2025). Antimicrobial activity and phytochemical profiling of natural plant extracts for biological control of wash water in the agri-food industry. Applied Sciences, 15: 5199. DOI: https://www.doi.org/10.3390/app15095199

Kar B, Kundu CN, Pati S, and Bhattacharya D (2023). Discovery of phyto-compounds as novel inhibitors against *NDM-1* and *VIM-1* protein through virtual screening and molecular modelling. Journal of Biomolecular Structure and Dynamics, 41(4): 1267-1280. DOI: https://www.doi.org/10.1080/07391102.2021.2019125

Kar P, Sharma NR, Singh B, Sen A, and Roy A (2021). Natural compounds from *Clerodendrum* spp. as possible therapeutic candidates against SARS-CoV-2: An *in silico* investigation. Journal of Biomolecular Structure and Dynamics, 39(13): 4774-4785. DOI: https://www.doi.org/10.1080/07391102.2020.1780947

Karagözlü N and Özeşer T (2024). Green synthesis, characterisation, and antibacterial activity of silver nanoparticles obtained from *Salvia officinalis* extract. Czech Journal of Food Sciences, 42(3): 163-173. DOI: https://www.doi.org/10.17221/4/2024-CJFS

Kathole KS, Hatwar PR, Bakal RL, and Karule VG (2025). Nano technology-based drug delivery systems and herbal medicine. Journal of Drug Delivery and Therapeutics, 15(3): 133-141. DOI: https://www.doi.org/10.22270/jddt.v15i3.7017

Kazi RNA, Hasani IW, Khafaga DSR, Kabba S, Farhan M, Aatif M, Muteeb G, and Fahim YA (2025). Nanomedicine: The Effective Role of Nanomaterials in Healthcare from Diagnosis to Therapy. Pharmaceutics, 17(8): 987. DOI: https://www.doi.org/10.3390/pharmaceutics17080987

Ke CL, Deng FS, Chuang CY, and Lin CH (2021). Antimicrobial actions and applications of chitosan. Polymers, 13(6): 904. DOI: https://www.doi.org/10.3390/polym13060904

Khan SA and Lee TKW (2022). Network-pharmacology-based study on active phytochemicals and molecular mechanism of *Cnidium monnieri* in treating hepatocellular carcinoma. International Journal of Molecular Sciences, 23(10): 5400. DOI: https://www.doi.org/10.3390/ijms23105400

Khanmohammadi M, Elmizadeh H, and Ghasemi K (2015). Investigation of size and morphology of chitosan nanoparticles used in drug delivery system employing chemometric technique. Iranian Journal of Pharmaceutical Research, 14(3): 665-675. Available at: https://pmc.ncbi.nlm.nih.gov/articles/PMC4518095/pdf/ijpr-14-665.pdf

Khatoon N, Alam Z, Hussain I, Khubaib B, Javed MA, and Ali Q (2024). Comprehensive analysis of *Seriphidium kurramense*: GC/MS profiling, antibacterial and antibiofilm activities, molecular docking study and *in-silico* ADME profiling. Discover Applied Sciences, 6(3): 107. DOI: https://www.doi.org/10.1007/s42452-024-05761-0

Konappa N, Udayashankar AC, Krishnamurthy S, Pradeep CK, Chowdappa S, and Jogaiah S (2020). GC-MS analysis of phytoconstituents from *Amomum nilgiricum* and molecular docking interactions of bioactive serverogenin acetate with target proteins. Scientific Reports, 10(1): 16438. DOI: https://www.doi.org/10.1038/s41598-020-73442-0

Kolahalam LA, Viswanath IK, Diwakar BS, Govindh B, Reddy V, and Murthy YLN (2019). Review on nanomaterials: Synthesis and applications. Materials Today: Proceedings, 18: 2182-2190. DOI: https://www.10.1016/j.matpr.2019.07.371

Krishnaveni B and Ragunathan R (2015). Extraction and characterization of chitin and chitosan from F. solani CBNR BKRR, synthesis of their bionanocomposites and study of their productive application. Journal of Pharmaceutical Sciences and Research, 7(4): 197-205. DOI: https://www.doi.org/10.35652/IGJPS.2015.22

Kumari P, Kumari C, and Singh PS (2017). Phytochemical screening of selected medicinal plants for secondary metabolites. International Journal of Life- Sciences Scientific Research, 3(4): 1151-1157. DOI: https://www.doi.org/10.21276/ijlssr.2017.3.4.9

Lazar V, Oprea E, and Ditu LM (2023). Resistance, tolerance, virulence and bacterial pathogen fitness—Current state and envisioned solutions for the near future. Pathogens, 12(5): 746. DOI: https://www.10.3390/pathogens12050746

Lokhande KB, Pawar SV, Madkaiker S, Nawani N, Venkateswara SK, and Ghosh P (2023). High throughput virtual screening and molecular dynamics simulation analysis of phytomolecules against BfmR of *Acinetobacter baumannii*: Anti-virulent drug development campaign. Journal of Biomolecular Structure and Dynamics, 41(7): 2698-2712. DOI: https://www.doi.org/10.1080/07391102.2022.2038271

López-León T, Carvalho ELS, Seijo B, Ortega-Vinuesa JL, and Bastos-González D (2005). Physicochemical characterization of chitosan nanoparticles: Electrokinetic and stability behavior. Journal of Colloid and Interface Science, 283(2): 344-351. DOI: https://www.doi.org/10.1016/j.jcis.2004.08.186

Mah TF (2014). Establishing the minimal bactericidal concentration of an antimicrobial agent for planktonic cells (MBC-P) and biofilm cells (MBC-B). Journal of Visualized Experiments, 83: 50854. DOI: https://www.doi.org/10.3791/50854

Maheswari BU and Kalaiselvi G (2024). Exploring neophytadiene from *Ampelocissus araneosa*: A molecular docking approach to inhibit biofilm formation in *Staphylococcus aureus*. Uttar Pradesh Journal of Zoology, 45(3): 59-70. DOI: https://www.doi.org/10.56557/upjoz/2024/v45i33875

Mendes FSF, Garcia LM, Moraes TS, Casemiro LA, Alcântara CB, Ambrósio SR, Veneziani RCS, Miranda MLD, and Martins CHG (2020). Antibacterial activity of *Salvia officinalis* L. against periodontopathogens: An *in vitro* study. Anaerobe, 63: 102194. DOI: https://www.doi.org/10.1016/j.anaerobe.2020.102194

Mohamed EM, Elmaidomy AH, Farhan SM, Abou-Zied HA, Bedaiwi RI, Alsenani F, Rabeh MA, Abbas GM, Abdelmohsen UR, and Zarka MA (2025). Antimicrobial potential of *Citrus australasica F. Muell*. Against methicillin-resistant *Staphylococcus aureus* supported by *in silico* analysis. Scientific Reports, 15(1): 17474. DOI: https://www.doi.org/10.1038/s41598-025-88113-1

Naskar S, Kuotsu K, and Sharma S (2019). Chitosan-based nanoparticles as drug delivery systems: A review on two decades of research. Journal of Drug Targeting, 27(4): 379-393. DOI: https://www.doi.org/10.1080/1061186X.2018.1512112

Noumi E, Ahmad I, Adnan M, Merghni A, Patel H, Haddaji N, Bouali N, Alabbosh KF, Ghannay S, Aouadi K et al. (2023). GC/MS Profiling, antibacterial, anti-quorum sensing, and antibiofilm properties of *Anethum graveolens L.* essential oil: Molecular docking study and *in-silico* ADME profiling. Plants, 12(10): 1997. DOI: https://www.doi.org/10.3390/plants12101997

Obanda BA, Gibbons CL, Fèvre EM, Bebora L, Gitao G, Ogara W, Wang SH, Gebreyes W, Ngetich R, Blane B et al. (2022). Multi-drug resistant *Staphylococcus aureus* carriage in abattoir workers in Busia, Kenya. Antibiotics, 11(12): 1726. DOI: https://www.doi.org/10.3390/antibiotics11121726

Omoshaba EO, Ojo OE, Oyekunle MA, Sonibare AO, and Adebayo AO (2020). Methicillin-resistant *Staphylococcus aureus* (MRSA) isolated from raw milk and nasal swabs of small ruminants in Abeokuta, Nigeria. Tropical Animal Health and Production, 52(5): 2599-2608. DOI: https://www.doi.org/10.1007/s11250-020-02301-x

Parida UK, Rout N, and Bindhani BK (2013). *In vitro* properties of chitosan nanoparticles induce apoptosis in human lymphoma SUDHL-4 cell line. Advances in Bioscience and Biotechnology, 4(12): 1118-1127. DOI: https://www.doi.org/10.4236/abb.2013.412148

Patel D, Aanchal, and Mohd AT (2024). Phytochemical and pharmacological aspects of *Salvia officinalis*. International Journal of of Novel Research and Development, 9(4): 442-452. Available at: https://ijnrd.org/papers/IJNRD2404157.pdf

Patel P, Vedarethinam V, Korsah MA, Danquah MK, and Jeevanandam J (2024). Exploring the potential of nanoparticles in the treatment of breast cancer: Current applications and future directions. Applied Sciences, 14(5): 1809. DOI: https://www.doi.org/10.3390/app14051809

Portia O, Leonard MK, and Aggrey BN (2024). *In vitro* antifungal potential of citral and nanoencapsulated citral against *Fusarium oxysporum f.sp. Lycopersici*. African Journal of Biotechnology, 23(4): 131-141. DOI: https://www.doi.org/10.5897/AJB2024.17662

Pouline SL, Murugesan S, and Raj TLS (2024). Anti-biofilm activity of *Barleria acanthoides* vahl against methicillin-resistant *Staphylococcus aureus*. Current Botany, 15: 157-163. DOI: https://www.doi.org/10.25081/cb.2024.v15.9184

Randhawa MA, Bawadekji A, Al Ali M, and Basha J (2018). Methanolic extract of *Salvia officinalis L*. (Maramia) possesses antimicrobial activity against MRSA, *Enterococcus faecalis*, multidrug resistant *Acinetobacter baumannii* and *Candida albicans*. Proceedings for Annual Meeting of the Japanese Pharmacological Society, WCP2018: PO1-9-21. DOI: https://www.doi.org/10.1254/jpssuppl.WCP2018.0_PO1-9-21

Rao A, Kumari S, Laura JS, and Dhania G (2023). Qualitative phytochemical screening of medicinal plants using different solvent extracts. Oriental Journal of Chemistry, 39(3): 621-626. DOI: https://www.doi.org/10.13005/ojc/390312

Rosado PC, Marques MM, and Justino GC (2025). Targeting MRSA penicillin-binding protein 2a: Structural insights, allosteric mechanisms, and the potential of adjuvant inhibitors. Biochemical Pharmacology, 239: 117048. DOI: https://www.doi.org/10.1016/j.bcp.2025.117048

Rudhani I (2018). *In vitro* antibacterial properties of ethanol extract from *Salvia Officinalis* (*L*.) plant growing wild in Kosovo. Biomedical Journal of Scientific and Technical Research, 2(3): 2578-2580. DOI: https://www.doi.org/10.26717/BJSTR.2018.02.000747

Rahdari M, Sadat Hashemi H, Hashemi SMA, Nadjafi-Semnani A, Jamalie S, Sakhaee MH, Zabihi F, Shariat Razavi SA, Taghdisi Khaboushan M, and Ahmadi G (2023). Advancements in the utilization of metal nanoparticles for breast cancer treatment: An *in vivo study* update. Journal of Lab Animal Research, 2(5): 63-71. DOI: https://www.doi.org/10.58803/jlar.v2i5.31

Saka A, Dey SR, Jule LT, Krishnaraj R, Dhanabal R, Mishra N, and Nagaprasad N (2024). Investigating antibacterial activity of biosynthesized silver oxide nanoparticles using *Phragmanthera Macrosolen L.* leaf extract. Scientific Reports, 14(1): 26850. DOI: https://www.doi.org/10.1038/s41598-024-75254-y

Salam Md A, Al-Amin Md Y, Salam MT, Pawar JS, Akhter N, Rabaan AA, and Alqumber MAA (2023). Antimicrobial resistance: A growing serious threat for global public health. Healthcare, 11(13): 1946. DOI: https://www.doi.org/10.3390/healthcare11131946

Samadian H, Salami MS, Jaymand M, Azarnezhad A, Najafi M, Barabadi H, and Ahmadi A (2020). Genotoxicity assessment of carbon-based nanomaterials: Have their unique physicochemical properties made them double-edged swords?. Mutation Research/Reviews in Mutation Research, 783: 108296. DOI: https://www.doi.org/10.1016/j.mrrev.2020.108296

Sanapalli V, Sanapalli BKR, and Mohammed AA (2025). Synthesis and antibacterial evaluation of an indole triazole conjugate with in silico evidence of allosteric binding to penicillin-binding protein 2a. Pharmaceutics, 17(8): 1013. DOI: https://www.doi.org/10.3390/pharmaceutics17081013

Sathiyabama M, Boomija RV, Muthukumar S, Gandhi M, Salma S, Prinsha TK, and Rengasamy B (2024). Green synthesis of chitosan nanoparticles using tea extract and its antimicrobial activity against economically important phytopathogens of rice. Scientific Reports, 14(1): 7381. DOI: https://www.doi.org/10.1038/s41598-024-58066-y

Selim S, Almuhayawi MS, Alqhtani H, Al Jaouni SK, Saleh FM, Warrad M, and Hagagy N (2022). Anti-*Salmonella* and antibiofilm potency of *Salvia officinalis L.* essential oil against antibiotic-resistant *Salmonella enterica.* Antibiotics, 11(4): 489. DOI: https://www.doi.org/10.3390/antibiotics11040489

Setiawansyah A and Gemantari BM (2022). Potential activity of caryophyllene derivatives as xanthine oxidase inhibitor: An *in silico* quantitative structure-activity relationship analysis. Journal of Food and Pharmaceutical Sciences, 3: 700-708. DOI: https://www.doi.org/10.22146/jfps.5485

Shalini K, Guleria S, Salaria D, Rolta R, Fadare OA, Mehta J, Awofisayo O, Mandyal P, Shandilya P, Kaushik N et al. (2024). Antimicrobial potential of phytocompounds of *Acorus calamus: In silico* approach. Journal of Biomolecular Structure and Dynamics, 42(5): 2726-2737. DOI: https://www.doi.org/10.1080/07391102.2023.2209653

Sharma K, Somavarapu S, Colombani A, Govind N, and Taylor KMG (2013). Nebulised siRNA encapsulated crosslinked chitosan nanoparticles for pulmonary delivery. International Journal of Pharmaceutics, 455(1-2): 241-247. DOI: https://www.doi.org/10.1016/j.ijpharm.2013.07.024

Sharma V, Gogoi B, Borah SN, Ghosh A, Mazumdar A, and Kalita RD (2025). *In-silico* molecular docking and molecular dynamic simulation of γ-elemene and caryophyllene identified from the essential oil of *Kaempferia galanga* L. against biofilm forming proteins, CrtM and SarA of *Staphylococcus aureus*. Journal of Biomolecular Structure and Dynamics, 43(15): 8357-8369. DOI: https://www.doi.org/10.1080/07391102.2024.2310773

Shidiki A and Vyas A (2022). Molecular docking and pharmacokinetic prediction of phytochemicals from *Syzygium cumini* in interaction with penicillin-binding protein 2a and erythromycin ribosomal methylase of *Staphylococcus aureus*. Biotechnologia, 103(1): 5. DOI: https://www.10.5114/bta.2022.113910

Swain A and Pan A (2025). Analysis of natural compounds identifies potential inhibitors for phosphoglucomutase of *Acinetobacter baumannii:* A computational approach. In Silico Pharmacology, 13(2): 76. DOI: https://www.doi.org/10.1007/s40203-025-00360-2

Tabassum R, Kousar S, Mustafa G, Jamil A, and Attique SA (2023). *In Silico* method for the screening of phytochemicals against methicillin-resistant *Staphylococcus aureus*. BioMed Research International, 2023(1): 5100400. DOI: https://www.doi.org/10.1155/2023/5100400

Tiwari H, Gupta P, Verma A, Singh S, Kumar R, Gautam HK, and Gautam V (2024). Advancing era and rising concerns in nanotechnology-based cancer treatment. ACS Chemical Health and Safety, 31(2): 153-161. DOI: https://www.doi.org/10.1021/acs.chas.3c00104

Tram G, Poole J, Adams FG, Jennings MP, Eijkelkamp BA, and Atack JM (2021). The *Acinetobacter baumannii* autotransporter adhesin ata recognizes host glycans as high-affinity receptors. ACS Infectious Diseases, 7(8): 2352-2361. DOI: https://www.doi.org/10.1021/acsinfecdis.1c00021

Verma AK, Ahmed SF, Hossain MS, Bhojiya AA, Mathur A, Upadhyay SK, and Bahadur NM (2022). Molecular docking and simulation studies of flavonoid compounds against PBP-2a of methicillin-resistant *Staphylococcus aureus*. Journal of Biomolecular Structure and Dynamics, 40(21): 10561-10577. DOI: https://www.10.1080/07391102.2021.1944911

Vinutha M, Manikandan A, Lakshmikanth RN, Shravani S, Divyashree B, Aishwarya K, and Nagaraj MM (2025). Molecular docking and anti-MRSA effects of bioactive compounds from Cymbopogon. *In Silico* Pharmacology, 13(2): 73. DOI: https://www.doi.org/10.1007/s40203-025-00334-4

WHO Bacterial Priority Pathogens List (2024). Bacterial pathogens of public health importance, to guide research, development, and strategies to prevent and control antimicrobial resistance. World health organization, Geneva, pp. 4-009346. Available at: https://www.who.int/publications/i/item/9789240093461

World health organization (WHO) (2022). Global antimicrobial resistance and use surveillance system (GLASS) report 2022. World Health Organization. Available at: https://www.who.int/initiatives/glass

Yahaya U, Sani Lawal M, Abubakar S, Rafiu Adeyemi S, Abdullahi Idris R, and Ibrahim Saad F (2020). Phytochemical Screening of Some Selected Nigerian Medicinal Plants. International Journal of Bioorganic Chemistry, 5(1): 1. DOI: https://www.doi.org/10.11648/j.ijbc.20200501.11

Zhang J, Li B, and Wang Q (2017). Application of Fourier transform infrared spectroscopy with chemometrics on postmortem interval estimation based on pericardial fluids. Scientific Reports, **7**: 18013. DOI: https://www.doi.org/10.1038/s41598-017-18228-7